Nationaal Lucht- en Ruimtevaartlaboratorium
National Aerospace Laboratory NLR

NLR-TP-2003-490

Electron Back Scatter Diffraction (EBSD) of corrosion, deformation and precipitation in the Gundestrup Cauldron

R.J.H. Wanhill, T. Hattenberg and J.P. Northover*

* University of Oxford

This report is intended for submission as a paper to Metal 2004: Triennial Metals Conservation Conference, in Canberra, Australia, October 2004.

This report may be cited on condition that full credit is given to NLR and the authors.

Customer:	National Aerospace Laboratory NLR
Working Plan number:	S.1.B
Owner:	National Aerospace Laboratory NLR
Division:	Structures and Materials
Distribution:	Unlimited
Classification title:	Unclassified
	October 2003

Approved by author:	Approved by project manager:	Approved by project managing department:
29/10/2003	31/10	31/10

Contents

2 Tables
11 Figures

(23 pages in total)

Electron Back Scatter Diffraction (EBSD) of Corrosion, Deformation and Precipitation in the Gundestrup Cauldron

R.J.H. Wanhill[1] , T. Hattenberg[1] and J.P. Northover [2]

Abstract

Electron backscatter diffraction (EBSD) was used to study samples from the Gundestrup Cauldron, a masterpiece of European Iron Age silverwork. One sample was essentially uncorroded and deformation-free. Three others contained varying amounts of corrosion and cold-deformation. Another important difference was that the deformation-free sample showed grain boundary precipitation, proven by EBSD to be discontinuous precipitation. Because the samples had comparable compositions, the results indicate that remanent cold-deformation was much more detrimental to corrosion resistance than discontinuous precipitation. This has implications for conservation, in that artefacts and parts of artefacts containing remanent cold-deformation will likely be more damaged by corrosion, and more susceptible to continuing damage. Another significant result, contrary to previous suggestions, is that the discontinuous precipitation characteristics cannot be used to determine the age, and hence authenticity, of silver artefacts.

Keywords: ancient silver, corrosion, cold-deformation, precipitation

Introduction

Automated electron backscatter diffraction (EBSD) has become available in the last decade. Used with a scanning electron microscope, EBSD is a powerful technique for microstructural analysis, including crystallographic texture, grain orientations and shapes, grain boundary and other boundary characteristics, deformation microstructures and phase identification. In the present study EBSD has been used, combined with a field emission gun scanning electron microscope (FEG SEM), to analyse small samples from the Gundestrup Cauldron. The results are directly relevant to conservation of ancient silver, and there are other implications too.

The Gundestrup Cauldron

Figure 1 shows the reassembled Gundestrup Cauldron, which is 69cm in diameter and 42cm high. It is the largest surviving silverwork from the European Iron Age, dating to the 2nd or 1st century BCE, and was found dismantled in a peat bog in Denmark in 1891. Owing to its size, high quality workmanship and iconographic variety, the Cauldron has been the subject of many studies, particularly about its origin, which is still controversial.

[1] National Aerospace Laboratory NLR, Amsterdam, The Netherlands
[2] Department of Materials, University of Oxford, Oxford, UK

The Cauldron consists of twelve plates and a bowl of 95-98% silver. Chemical analysis shows comparable compositions, with copper as the main, and varying, impurity element. This limited variation in composition is useful for archaeometallurgical studies.

Experimental Information

Four small samples taken from different parts of the Gundestrup Cauldron and embedded in a conducting resin were prepared for metallography by standard polishing and etching methods. The etchant was ammoniacal hydrogen peroxide. The samples were examined using a FEG SEM equipped with EBSD. As indicated in the introduction to this paper, the EBSD technique provides many analysis options. We found the following options of most use:

- Inverse pole figure (IPF) colour coded maps.
- Pole figures (PF) and inverse pole figures (IPF).
- Boundary rotation angle maps.
- Coincidence site lattice (CSL) maps.

Chemical analyses (wt.%)

The samples had the following compositions:

Sample	Cu	Au	Pb	Bi	Traces
361	4.64	0.29	0.39	0.07	Fe,Ni
363	1.76	0.35	0.52	0.13	Fe,Zn
365	2.17	0.33	0.58	0.11	Fe,Ni,Zn
366	3.44	0.36	0.64	0.11	Fe,Ni,Zn

Apart from the copper contents the samples had fairly similar amounts of other elements.

EBSD of sample 366

SEM imaging showed this sample to be virtually free of corrosion and cold-deformation, i.e. it had not undergone further mechanical processing after a final annealing heat-treatment. The EBSD analyses are shown in figures 2-4, and their interpretation is given in table 1. The most significant results are a random microtexture and extensive precipitation at grain boundaries. Figure 4 compares details of figure 2a, the IPF colour coded map, with SEM images. These comparisons demonstrate that the precipitation is the type known as discontinuous[*] precipitation (Smith 1953; Williams and Edington 1976; Gust 1979; Doherty 1996). The precipitation is due to copper, first shown by Fraenkel (1926) and Norbury (1928).

[*] The term "discontinuous" can be confusing. It refers to an abrupt change in alloy matrix composition, not the precipitate morphology

EBSD of samples 361, 363, 365

SEM imaging showed these samples to be damaged by corrosion and to contain remanent cold-deformation. The EBSD analyses are shown in figures 5-10, and their interpretation is given in table 2. The most significant results are increased corrosion damage, visible as cracking, with increased remanent cold-deformation, and no evidence of precipitation at grain boundaries. The corrosion-induced cracking occurred mainly at grain boundaries, but was also transcrystalline, as is best seen in figure 9a.

The link between corrosion and cold-deformation agrees with results from investigating an Egyptian silver vase (Wanhill *et al.* 1998) and re-interpretation of damage in an Indian silver coin (Thompson and Chatterjee 1954; Wanhill 2002). In particular, the Egyptian vase investigation showed that transcrystalline corrosion occurred along slip lines and deformation twin boundaries.

Discussion

Corrosion, deformation, precipitation and conservation

The present study indicates that remanent cold-deformation is much more detrimental to the corrosion resistance of ancient silver, *in casu* the Gundestrup Cauldron, than discontinuous precipitation. This is remarkable because the eminent metallurgist Cyril Stanley Smith opined that grain boundaries along which discontinuous precipitation has occurred seem to be highly susceptible to corrosion (Smith 1965). On the other hand, the present findings are consistent with previous work by one of us (JPN) on ancient Bactrian silver. This showed intergranular corrosion and cracking despite copper contents less than 1 wt.%, which is almost certainly too low for discontinuous precipitation to occur, even at above-ambient temperatures: see figure 10 in Wanhill (2002), which replots data by Ageew *et al.* (1930).

From the above it is evident that conservation of ancient silver should include assessment for remanent cold-deformation. Artefacts and parts of artefacts containing cold-deformation will likely be more damaged by corrosion, and more susceptible to continuing damage. Typical areas likely to contain cold-deformation are chased and stamped decorations, whereby it is noteworthy that for sheet-metal artefacts the *reverse* or *internal* sides may be more susceptible to corrosion (Wanhill *et al.* 1998; Wanhill 2002). Chasing and stamping can result in tensile strains on the reverse or internal sides, and these tensile strains promote corrosion that is analogous - or possibly identical - to a type of stress corrosion cracking (Wanhill 2002; Lichter *et al.* 2001).

Discontinuous precipitation

Several aspects of the discontinuous precipitation in silver are of archaeometallurgical and fundamental interest:

- Precipitate widths and morphology.
- Non-occurrence in samples containing remanent cold-deformation.
- Nucleation and growth.

(1) Precipitate widths and morphology. The discontinuous precipitation in sample 366 had widths up to 7µm and a finely-mottled appearance. Some precipitate widths were therefore well beyond 2µm, which is the maximum predicted for 2000 years of precipitation at ambient temperatures (Wanhill 2002). This prediction assumes Arrhenius-type reaction kinetics and requires extrapolation from experimental data obtained at temperatures of 200 °C and higher. Thus, either Arrhenius reaction kinetics do not apply to ambient temperature precipitation, or else the precipitation in sample 366 occurred at an elevated temperature. Neither possibility can be presently excluded.
The precipitate's finely mottled appearance is consistent with many other results, for both modern and ancient silver (Norbury 1928; Gayler and Carrington 1947; Rose 1957; Smith 1965; Leo 1967; Predel and Ruge 1968; Scharfenberger *et al.* 1972; Schweizer and Meyers 1978a, 1979).
Taken as a whole, the sample 366 precipitate widths and finely-mottled appearance refute a suggestion that the precipitate could be used to determine the age, and hence authenticity, of silver artefacts (Schweizer and Meyers 1978b, 1979). First, many of the precipitate widths were unpredictably large. Second, the precipitate does not form regular lamellae whose spacing might depend on the ageing temperature such that one could distinguish between genuine long-term precipitation at ambient temperatures and short-term precipitation at elevated temperatures (Schweizer and Meyers 1979).

(2) Non-occurrence in samples 361, 363 and 365. Experiments have shown that cold-deformation can reduce the growth rate, and hence width, of discontinuous precipitation in silver-copper alloys at elevated temperatures, and this could be due to deformation-induced continuous precipitation within the grains (Scharfenberger *et al.* 1972). A similar effect could have been operating in samples 361, 363 and 365 (note that sample 361 contains more copper than sample 366), even to the extent that discontinuous precipitation was prevented. However, verification of this will require transmission electron microscopy (TEM).

(3) Nucleation and growth. The nucleation and growth characteristics illustrated in figure 4 are hallmarks of discontinuous precipitation (Smith 1953; Williams and Edington 1976; Gust 1979; Doherty 1996). An interesting problem is how it is possible for discontinuous precipitation to grow in opposite directions from adjacent sites on the same grain boundary (Williams and Edington 1976; Doherty 1996). An explanation for aluminium-lithium alloys has been proposed (Williams and Edington 1976), but this cannot be a general one or applicable to silver-copper alloys.

Grain boundaries and grain sizes

Watanabe (1984,1993,1994) and Watanabe *et al.* (1980,1989) suggested dividing grain boundaries into three character-determined categories: low-angle boundaries with misorientation angles less than 15° ; high-angle CSL boundaries with low Σ coincidence (less than Σ29); and high-angle random boundaries. The basic distinguishing property is that low-angle and low Σ coincidence boundaries are low-energy boundaries, while random boundaries are high-energy boundaries.

This distinction between grain boundary types and structures is relevant to archaeological silver artefacts. These were usually made by combinations of mechanical working (cold-deformation) and annealing heat-treatments. The resulting microstructures would therefore be expected to contain a majority of high-angle random grain boundaries, by analogy with results for aluminium (Watanabe 1984) and iron-silicon alloys (Watanabe *et al.* 1989).

Figure 11 shows misorientation angle histograms for the Gundestrup Cauldron samples. The annealed sample 366 had an evident majority of high-angle misorientations. These corresponded mainly or entirely to high-angle random grain boundaries, since other EBSD measurements showed very few CSL boundaries apart from the Σ3 annealing twin boundaries. The samples 361, 363 and 365 had progressively decreasing *relative amounts* of high-angle misorientations, but this is because cold-deformation introduced many low-angle boundaries due to slip dislocations.

On balance, we may conclude that the sample grain boundaries were mainly high-angle random boundaries, as expected for most archaeological silver artefacts, see above. This evidence and general supposition lead to two potentially important consequences (Wanhill 2002). First, archaeological silver will contain many grain boundaries susceptible to impurity element segregation, including discontinuous precipitation of copper, but also possible segregation of microstructurally-embrittling elements such as lead and bismuth. Second, if the silver contains cracks, then the grain size is important.

In general, a large grain size is detrimental to archaeological silver embrittlement, whether it is due to corrosion or segregation of microstructurally-embrittling elements (Wanhill 2002). Figures 5a and 7a might seem to contradict this, since they show intensive corrosion-induced cracking in areas of small recrystallized grains. However, the damage is relatively superficial and does not penetrate deeply into the samples. This latter aspect is more important for the overall integrity of an artefact.

Conclusions

Two main conclusions can be drawn from automated electron backscatter diffraction (EBSD) analyses of samples from the Gundestrup Cauldron, a famous silver artefact over 2000 years old:

(1) Remanent cold-deformation was much more detrimental to the corrosion resistance than grain boundary discontinuous precipitation. Conservation of ancient silver should include assessment for remanent cold-deformation.

(2) The characteristics of discontinuous precipitation cannot be used to determine the age, and hence authenticity, of silver artefacts.

References

Ageew, N., Hansen, M., and Sachs, G., 1930, Entmischung und Eigenschaftänderungen übersättigter Silber-Kupferlegierungen, Zeitschrift für Physik, 66, 350-376.

Doherty, R.D., 1996, Diffusive phase transformations in the solid state, Chapter 15 in Physical Metallurgy (Editors R.W. Cahn and P. Haasen), Volume II, 1456-1458, Elsevier Science B.V., Amsterdam, The Netherlands.

Fraenkel, W., 1926, Zur Kenntnis der Vorgänge bei der Entmischung übersättigter Mischkristalle, Zeitschrift für Anorganische und Allgemeine Chemie, 154, 386-394.

Gayler, M.L.V., and Carrington, W.E., 1947, Metallographic study of the precipitation of copper from a silver-rich silver-copper alloy, Journal of the Institute of Metals, 73, 625-639.

Gust, W., 1979, Discontinuous precipitation in binary metallic systems, Phase Transformations, Volume II, II-27 - II-68, The Institution of Metallurgists, London, U.K.

Leo, W., 1967, Elektronenmikroskopische Untersuchungen zur Ausscheidung in aushärtbaren Silber-Kupfer-Legierungen, Zeitschrift für Metallkunde, 58, 456-461.

Lichter, B.D., Lu, H., and Flanagan, W.F., 2001, Strain-enhanced dissolution: a model for transgranular stress-corrosion cracking, in Proceedings of the 2nd International Conference on Environment Sensitive Cracking and Corrosion Damage (Editors M. Matsumura, H. Nagano, K. Nakasa and Y. Isomoto), 271-278, Nishiki Printing Ltd., Hiroshima, Japan.

Norbury, A.L., 1928, The effect of quenching and tempering on the mechanical properties of standard silver, Journal of the Institute of Metals, 39, 145-172.

Predel, B., and Ruge, H., 1968, Untersuchung der Kinetik der diskontinuierlichen Entmischung übersättigter Silber-Mischkristalle, Zeitschrift für Metallkunde, 59, 777-781.

Rose, R.G., 1957, The precipitation of copper from a silver-5.5% copper solid solution at 220 ºC, Acta Metallurgica, 5, 404-405.

Scharfenberger, W., Schmitt, G., and Borchers, H., 1972, Über die Kinetik der diskontinuierlichen Ausscheidung der Silberlegierung mit 7,5 Gew.-%Cu, Zeitschrift für Metallkunde, 63, 553-560.

Schweizer, F., and Meyers, P., 1978a, Structural changes in ancient silver alloys: the discontinuous precipitation of copper, Paper 78/23/5 in ICOM Committee for Conservation 5th Triennial Meeting, 1978, Zagreb, Yugoslavia.

Schweizer, F., and Meyers, P., 1978b, Authenticity of ancient silver objects: a new approach, MASCA Journal, 1, 9-10.

Schweizer, F., and Meyers, P., 1979, A new approach to the authenticity of ancient silver objects: the discontinuous precipitation of copper from a silver-copper alloy, in Proceedings of the 18th International Symposium on Archaeometry and Archaeological Prospection, Rheinland-Verlag GmbH, 287-298, Cologne, Germany.

Smith, C.S., 1953, Microstructure (1952 Edward deMille Campbell Memorial Lecture), Transactions of the American Society for Metals, 45, 533-575.

Smith, C.S., 1965, The interpretation of microstructures of metallic artifacts, in Application of Science in Examination of Works of Art (Editor W.J. Young), 20-52, Boston Museum of Fine Arts, Boston, Massachusetts, U.S.A.

Thompson, F.C., and Chatterjee, A.K., 1954, The age-embrittlement of silver coins, Studies in Conservation, 1, 115-126.

Wanhill, R.J.H., Steijaert, J.P.H.M., Leenheer, R., and Koens, J.F.W., 1998, Damage assessment and preservation of an Egyptian silver vase (300-200 BC), Archaeometry, 40, 123-137.

Wanhill, R.J.H., 2002, Archaeological silver embrittlement: a metallurgical inquiry, NLR Technical Publication NLR-TP-2002-224, National Aerospace Laboratory NLR, Amsterdam, The Netherlands.

Watanabe, T., 1984, An approach to grain boundary design for strong and ductile polycrystals, Res Mechanica, 11, 47-84.

Watanabe, T., 1993, Grain boundary design and control for high temperature materials, Materials Science and Engineering, A166, 11-28.

Watanabe, T., 1994, The impact of grain boundary character distribution on fracture in polycrystals, Materials Science and Engineering, A176, 39-49.

Watanabe, T., Fujii, H., Oikawa, H., and Arai, K.I., 1989, Grain boundaries in rapidly solidified and annealed Fe-6.5 mass % Si polycrystalline ribbons with high ductility, Acta Metallurgica, 37, 941-952.

Watanabe, T., Kitamura, S., and Karashima, S., 1980, Grain boundary hardening and segregation in alpha iron-tin alloy, Acta Metallurgica, 28, 455-463.

Williams, D.B., and Edington, J.W., 1976, The discontinuous precipitation reaction in dilute Al-Li alloys, Acta Metallurgica, 24, 323-332.

Table 1 EBSD analyses of sample 366

Analysis types	Figure numbers	Observations and interpretations
IPF colour coded map	2a	• random orientation equiaxed grains containing annealing twins • "black" ledges due to selective etching at precipitate boundaries
PF and IPF	2b	• random microtexture
Boundary rotation angle map	3a	• mainly 45° - 60° boundaries, mostly annealing twins; few low-angle (1° - 15°) boundaries
CSL map for Σ3 boundaries	3b	• Σ3 boundaries mostly annealing twins; grain boundaries and precipitates visible
IPF map / SEM image (details)	4	• precipitate nucleation and growth, diagnostic for discontinuous precipitation

Table 2 EBSD analyses of samples 361, 363 and 365

Analysis types	Figure numbers	Observations and interpretations
IPF colour coded map, PF and IPF	5a,5b	• random orientation equiaxed grains containing annealing twins; deformation-induced minor orientation changes within grains and twins
IPF colour coded maps, PFs and IPFs	7,9	• deformation-induced local texturing; annealing twins increasingly less visible
IPF colour coded maps	5a,7a,9a	• corrosion-induced cracking ("black"regions) mainly along grain boundaries and intensive in areas of small recrystallized grains, see figures 5a and 7a
Boundary rotation angle maps	6a,8a,10a	• increasing amounts of low-angle (1° - 15°) boundaries from deformation by slip
Boundary rotation angle maps and CSL maps for Σ3 boundaries	6,8,10	• increasing numbers of deformation twins (narrow, irregular pairs of yellow colour-coded boundaries)
CSL maps for Σ3 boundaries	6b,8b,10b	• grey-scale darkening of areas deformed by slip and twinning
IPF and boundary rotation angle maps	9a,10a	• corrosion-induced transcrystalline cracking, some along deformation twins

Fig. 1 The Gundestrup Cauldron

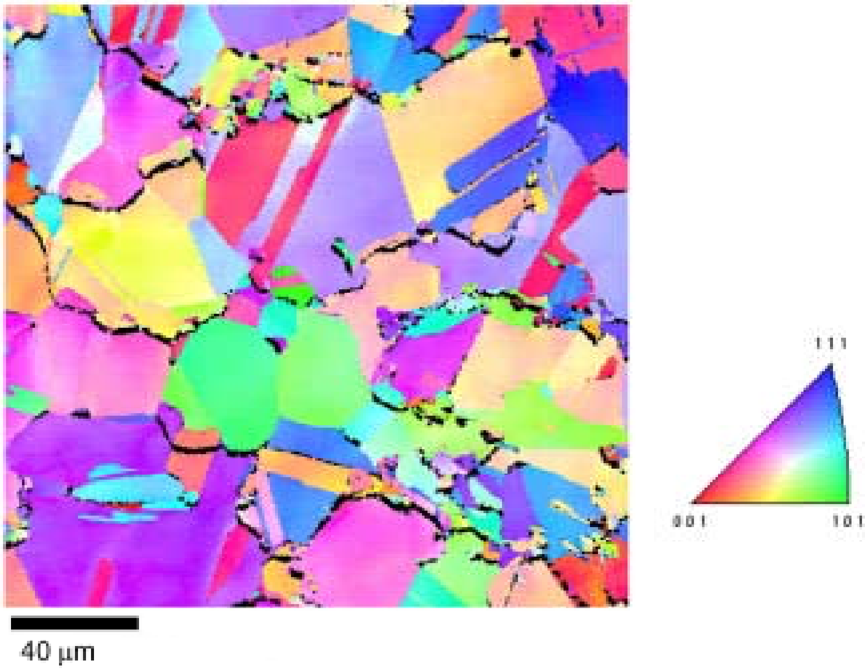

(a) Inverse pole figure (IPF) [001] colour coded map

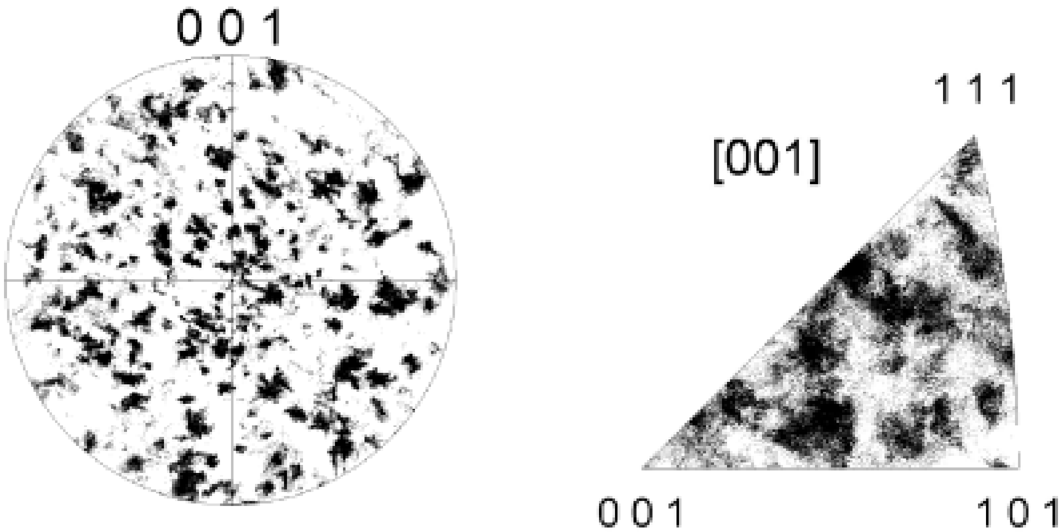

(b) Pole figure (PF) and inverse pole figure (IPF)

Fig. 2 Microtexture of sample 366

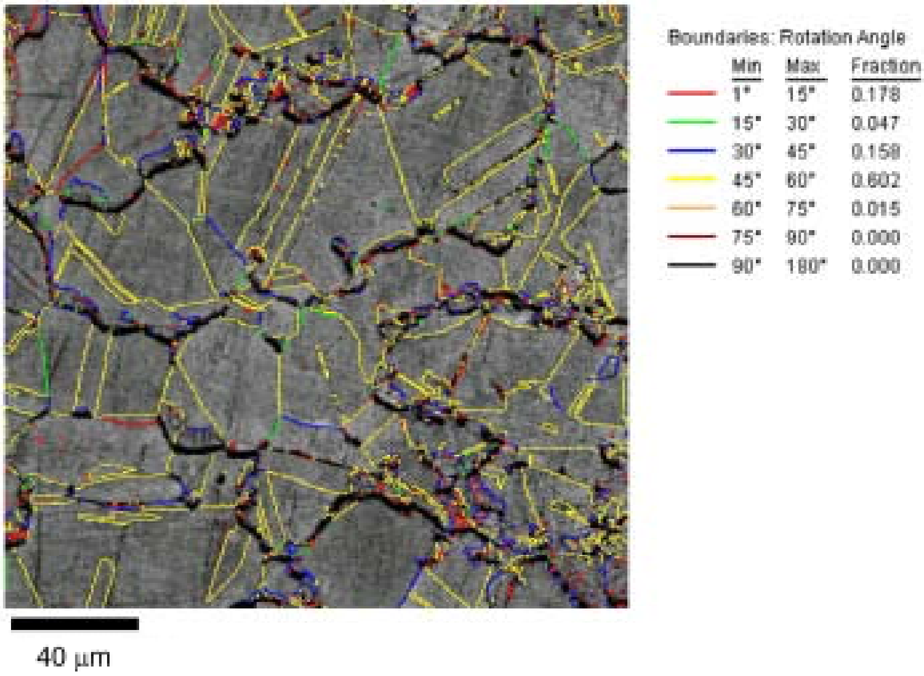

(a) Image quality (IQ) map with rotation angles

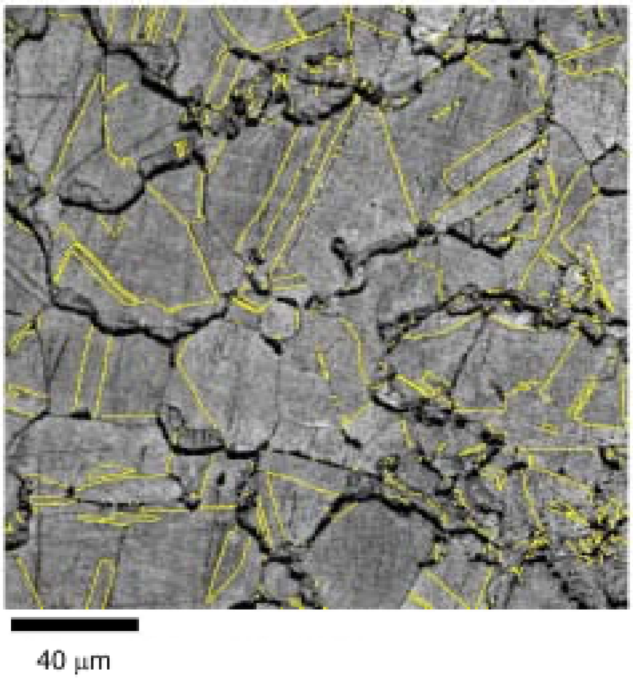

(b) Coincidence site lattice (CSL) map with Σ3 boundaries

Fig. 3 Boundary maps for sample 366

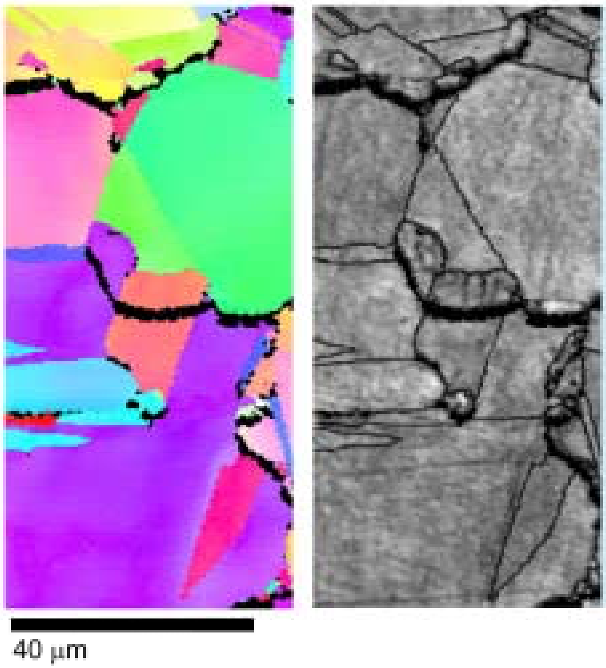

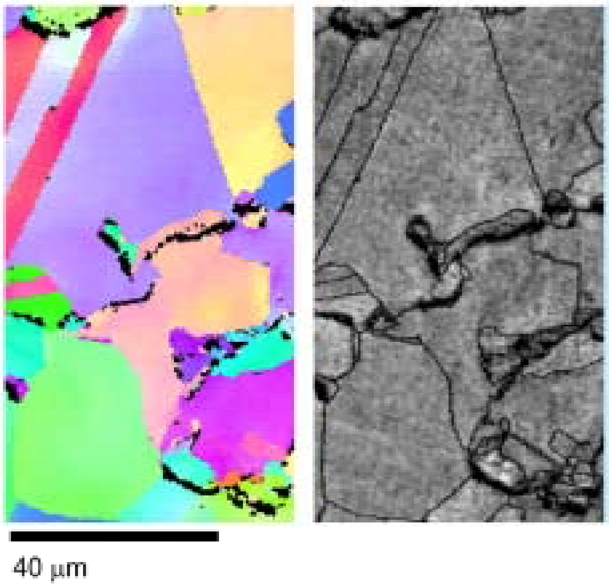

Fig. 4 Details of precipitate nucleation and growth in sample 366

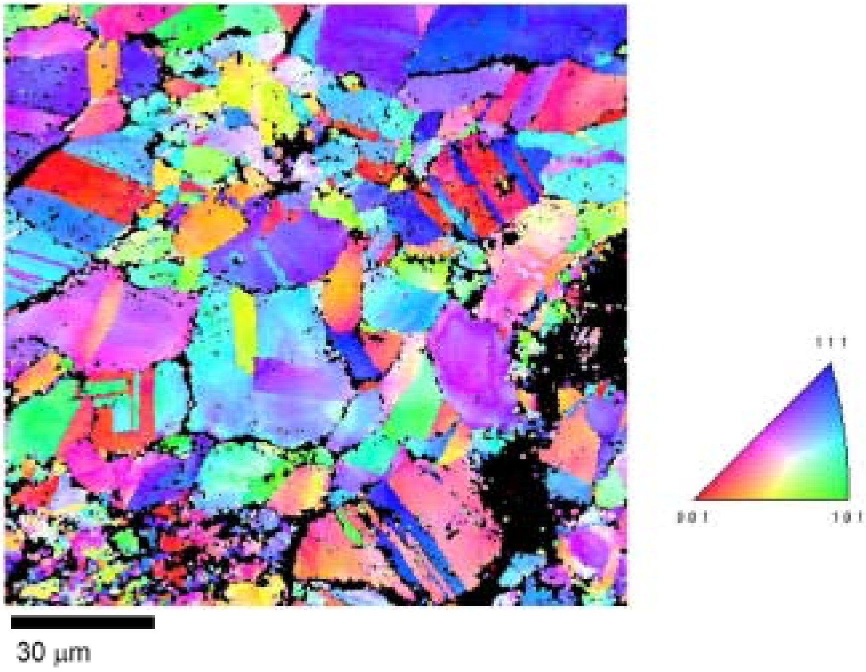

(a) Inverse pole figure (IPF) [001] colour coded map

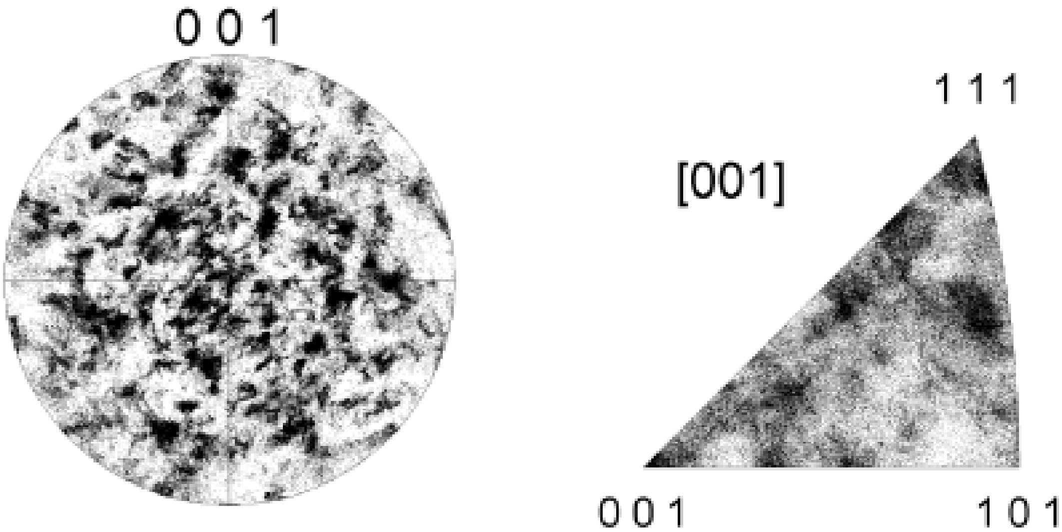

(b) Pole figure (PF) and inverse pole figure (IPF)

Fig. 5 Microtexture of sample 361

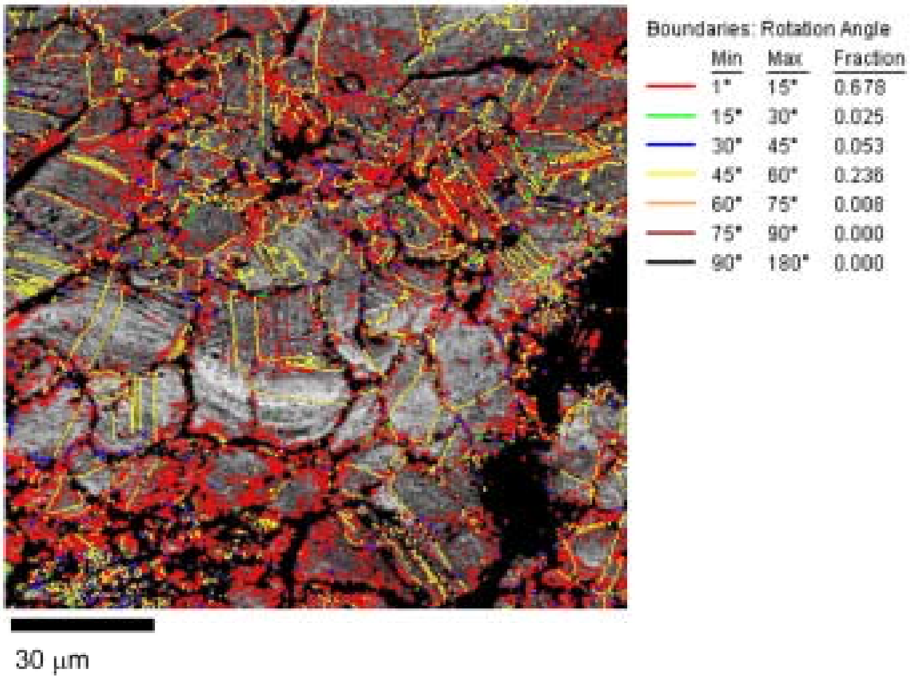

(a) Image Quality (IQ) map with rotation angles

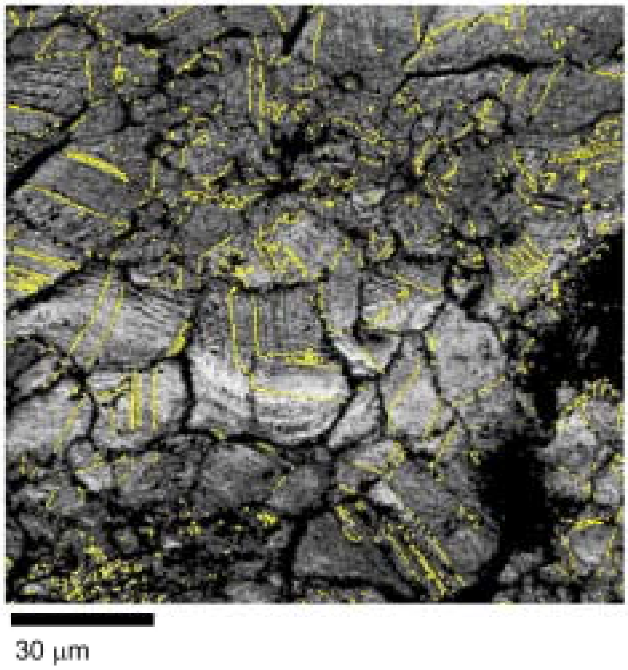

(b) Coincidence site lattice (CSL) map with Σ3 boundaries

Fig. 6 Boundary maps for sample 361

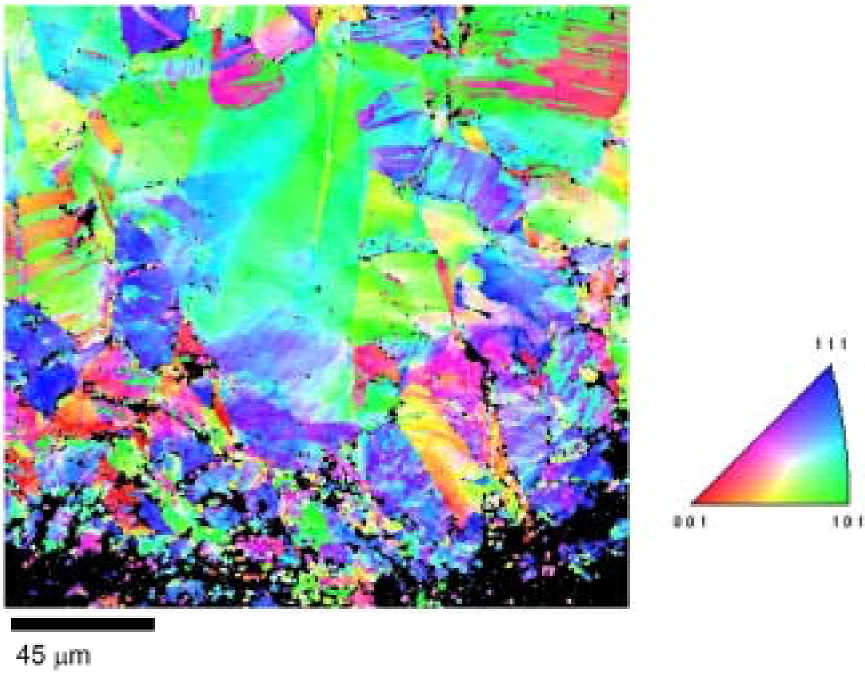

(a) Inverse pole figure (IPF) [001] colour coded map

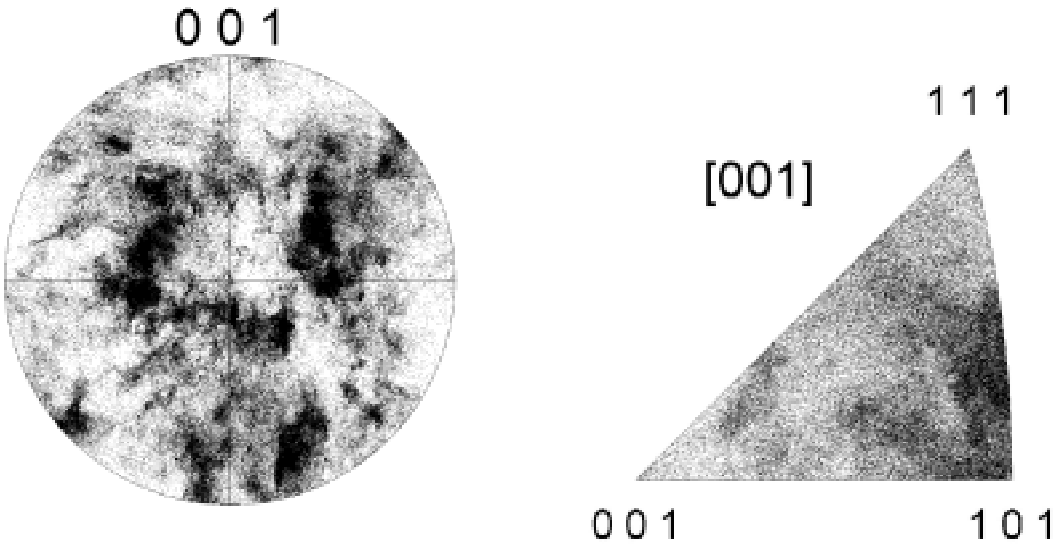

(b) Pole figure (PF) and inverse pole figure (IPF)

Fig. 7 Microtexture of sample 363

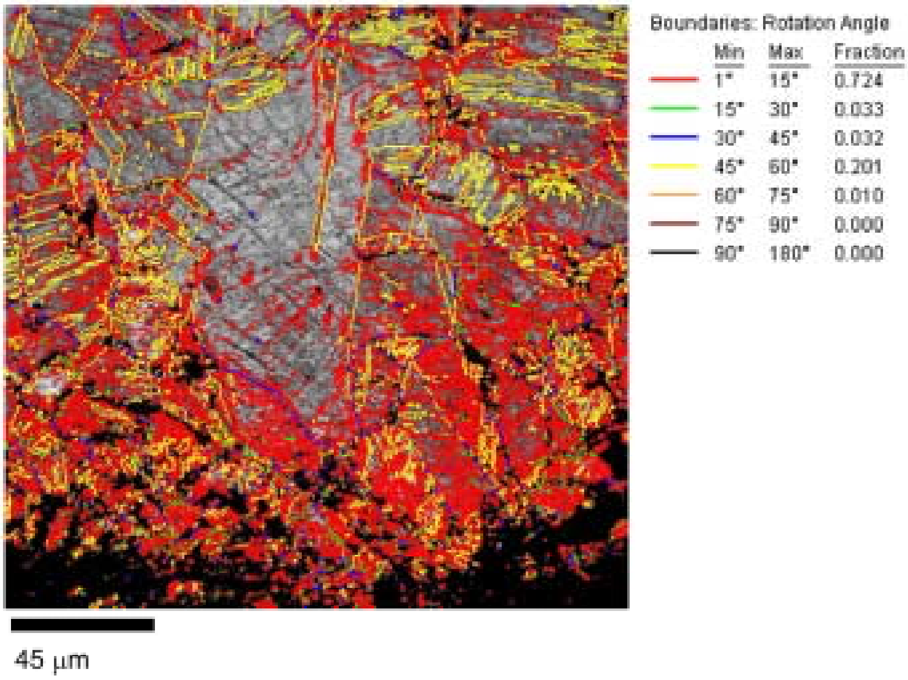

(a) Image Quality (IQ) map with rotation angles

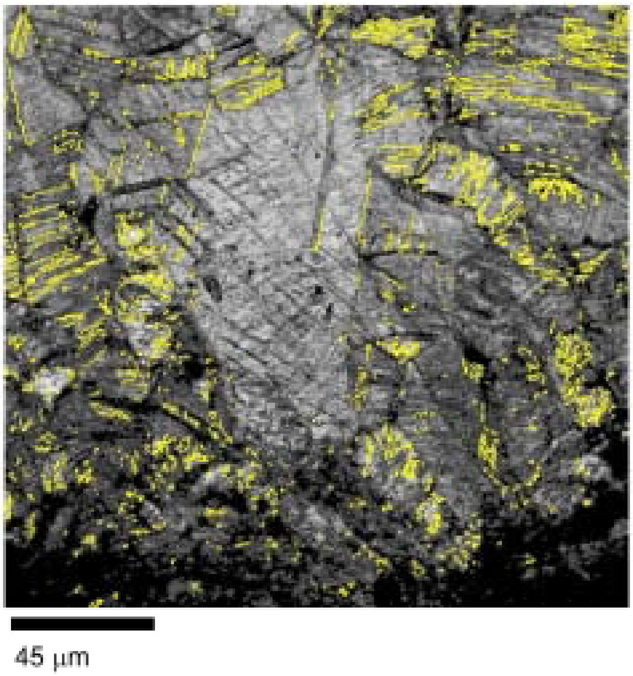

(b) Coincidence site lattice (CSL) map with Σ3 boundaries

Fig. 8 Boundary maps for sample 363

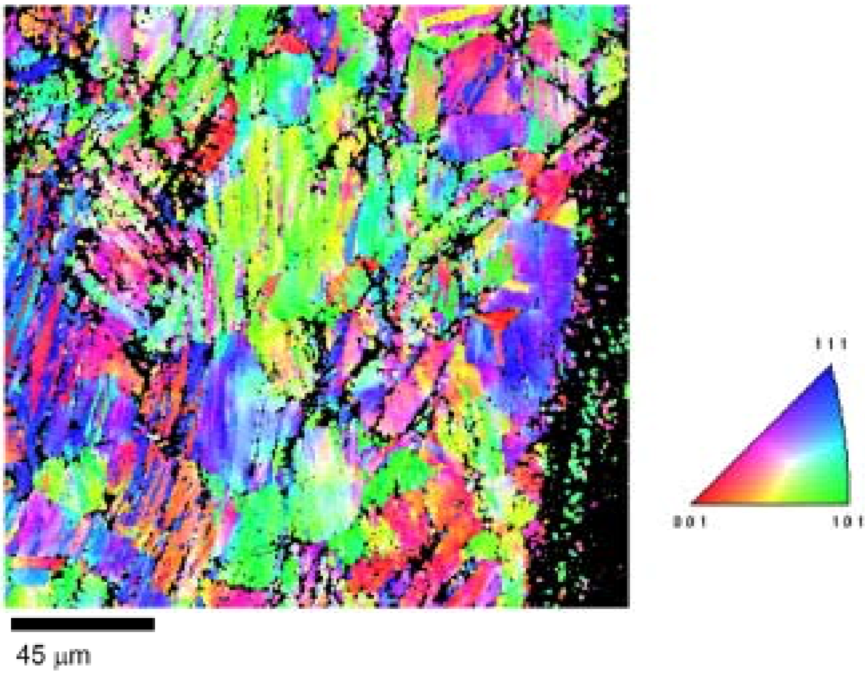

(a) Inverse pole figure (IPF) [001] colour coded map

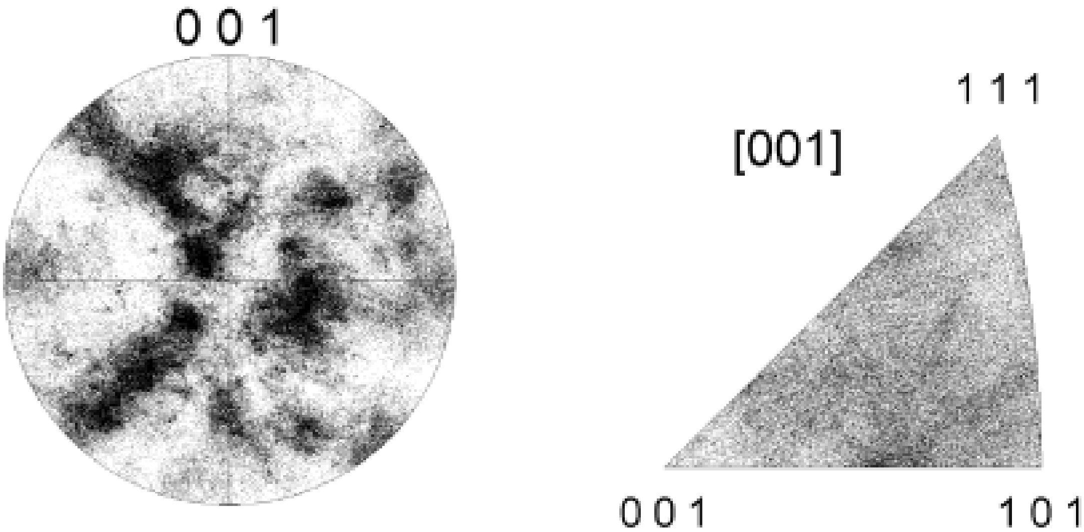

(b) Pole figure (PF) and inverse pole figure (IPF)

Fig. 9 Microtexture of sample 365

D593-01N

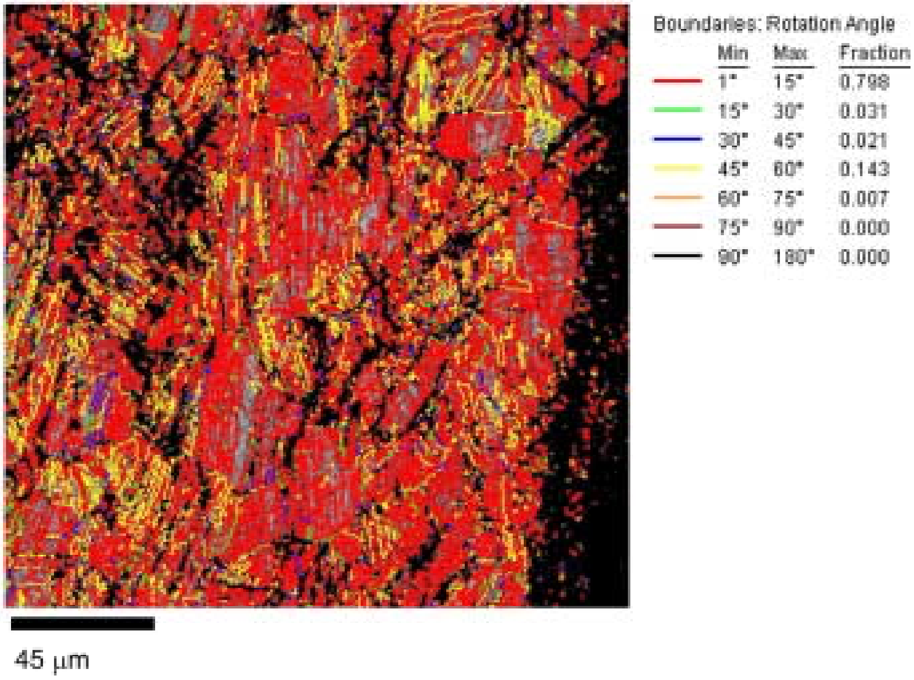

(a) Image Quality (IQ) map with rotation angles

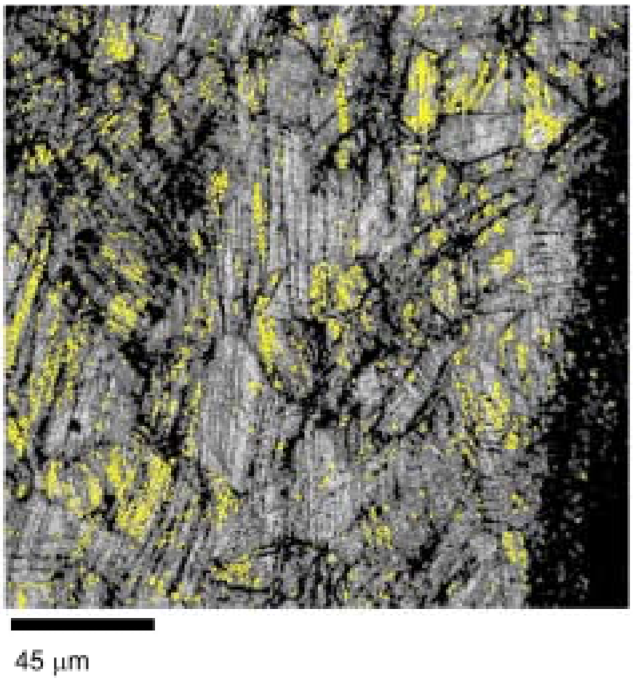

(b) Coincidence site lattice (CSL) map with Σ3 boundaries

Fig. 10 Boundary maps for sample 365

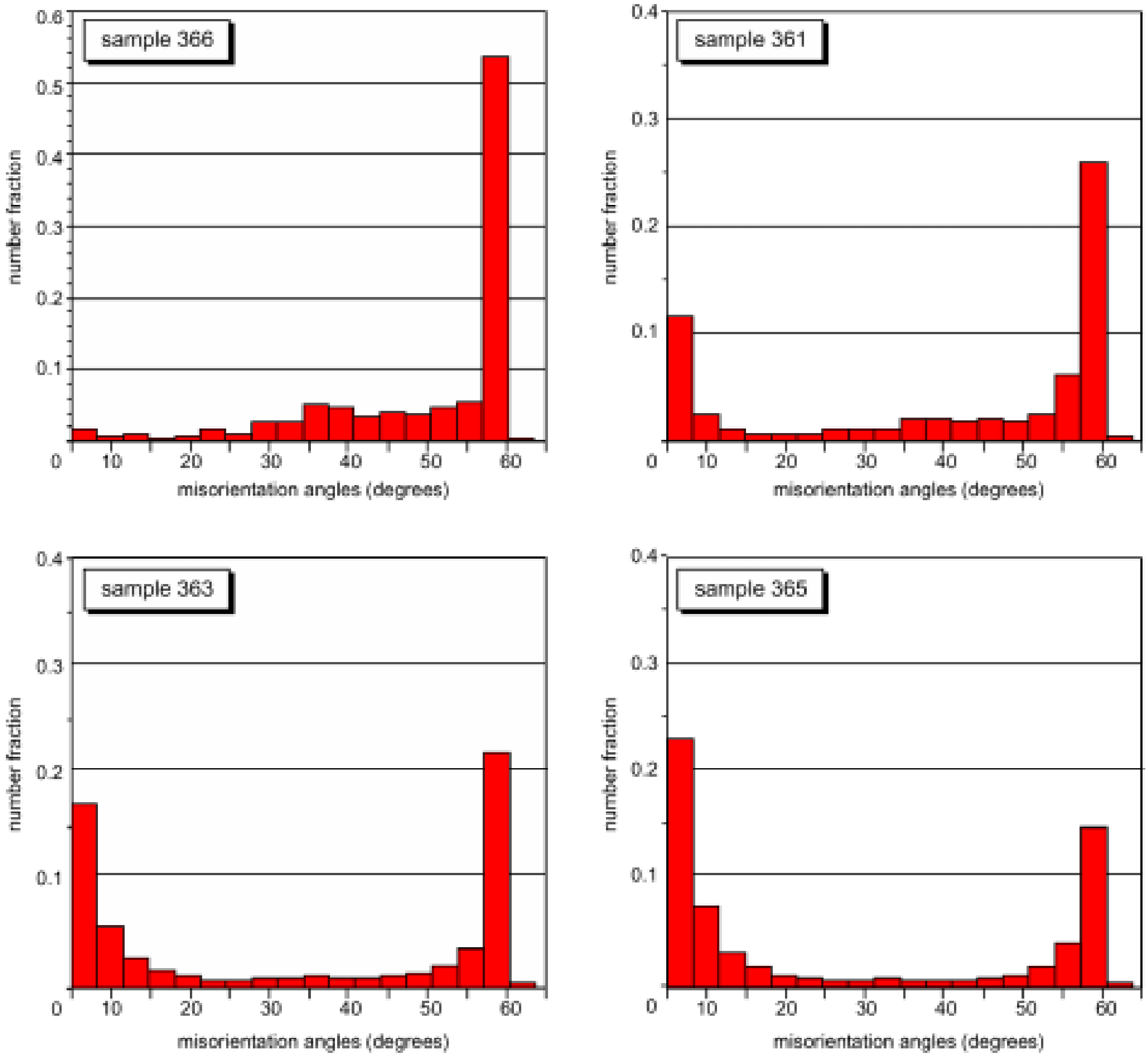

Fig. 11 Misorientation angle histograms for samples 366 (annealed) and 361, 363, 365 (remanent cold - deformation)